# Strain Control of Giant Magnetic Anisotropy in Metallic Perovskite SrCoO₃₋δ Thin Films

Songbai Hu,*[†,‡,#] Claudio Cazorla,[‡] Feixiang Xiang,[∥] Hongfei Ma,[†] Jianyuan Wang,[⊥] Jianbo Wang,[#] Xiaolin Wang,[∥] Clemens Ulrich,[§] Lang Chen,[†] and Jan Seidel*[‡]

[†]Department of Physics, South University of Science and Technology of China, Shenzhen 518055, China

[‡]School of Materials Science and Engineering and [§]School of Physics, UNSW Sydney, Sydney, NSW 2052, Australia

[∥]Spintronic and Electronic Materials Group, Institute for Superconducting and Electronic Materials, Australian Institute for Innovative Materials, University of Wollongong, Wollongong, NSW 2522, Australia
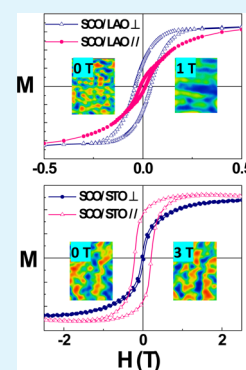
[⊥]School of Nature and Applied Science, Northwestern Polytechnical University, Xi'an 710072, China

[#]School of Physics and Technology, Wuhan University, Wuhan 430072, China

Ⓢ *Supporting Information*

**ABSTRACT:** Magnetic materials with large magnetic anisotropy are essential for workaday applications such as permanent magnets and magnetic data storage. There is widespread interest in finding efficient ways of controlling magnetic anisotropy, among which strain control has proven to be a very powerful technique. Here, we demonstrate the strain-mediated magnetic anisotropy in SrCoO₃₋δ thin film, a perovskite oxide that is metallic and adopts a cubic structure at $\delta \leq 0.25$. We find that the easy-magnetization axis in SrCoO₃₋δ can be rotated by 90° upon application of moderate epitaxial strains ranging from −1.2 to +1.8%. The magnetic anisotropy in compressive SrCoO₃₋δ thin films is huge, as shown by magnetic hysteresis loops rendering an anisotropy energy density of ∼$10^6$ erg/cm³. The local variance in magnetic force microscopy upon temperature and magnetic field reveals that the evolution of magnetic domains in the SCO thin film is strongly dependent on magnetic anisotropy.



**KEYWORDS:** *SrCoO₃₋δ thin films, epitaxial strain, magnetic anisotropy, MFM, DFT*

## 1. INTRODUCTION

Epitaxial strain has proven a very powerful technique for tuning and enhancing the functional properties of complex materials. Inherent to this success are the strong couplings between structural degrees of freedom and magnetic, electrical, orbital, and charge-order parameters. To date, control of magnetic anisotropy has been demonstrated in just a few complex oxides and semiconductor alloys synthesized as thin films.[1−8] Most of those materials, which could be used in advanced information processing and storage applications like spintronic devices, however, present impeding practical issues owing to their insulating nature. SrCoO₃₋δ is a perovskite oxide that undergoes a number of intriguing magnetic phase transitions driven by strain.[9−16] The magnetic properties of SCO present a strong dependence on oxygen stoichiometry and epitaxial strain conditions. Bulk stoichiometric SCO is ferromagnetic below 305 K,[17] and its Curie temperature, $T_c$, decreases linearly with $\delta$.[18] At $0 \leq \delta \leq 0.25$ SrCoO₃₋δ (SCO) adopts a simple cubic perovskite structure and is metallic (see the Supporting Information Figure S1).[10,19] In the brownmillerite phase ($\delta = 0.5$), bulk SrCoO₃₋δ is antiferromagnetic and its Neel temperature amounts to 570 K.[20] In the SCO thin films, a ferromagnetic−antiferromagnetic phase transition has been experimentally observed under tensile conditions[13] and

consistently reproduced with theoretical calculations.[9,16] The structural and chemical simplicity of SCO along with its controllable ferromagnetic and electrical conductivity properties, convert this material into an ideal candidate for developing new information-processing and storage technologies (e.g., spintronic devices). In spite of these encouraging prospects, the magnetic properties of strain-tuned, especially compressively strained SCO thin films remain mostly unknown to date.

In this work, we use a combination of experimental characterization techniques (e.g., X-ray diffraction (XRD), magnetic property measurement system (MPMS), magnetic force microscopy (MFM), and first principles simulation methods) to determine with atomic precision the magnetic structure of SCO thin films under moderate compressive and tensile epitaxial strains. We find yet unobserved giant perpendicular magnetic anisotropy (PMA) at moderate compressive conditions that sets a new record among the perovskite oxides with elemental formula ABO₃. The tunability of such a giant PMA is remarkable, as the associated anisotropy
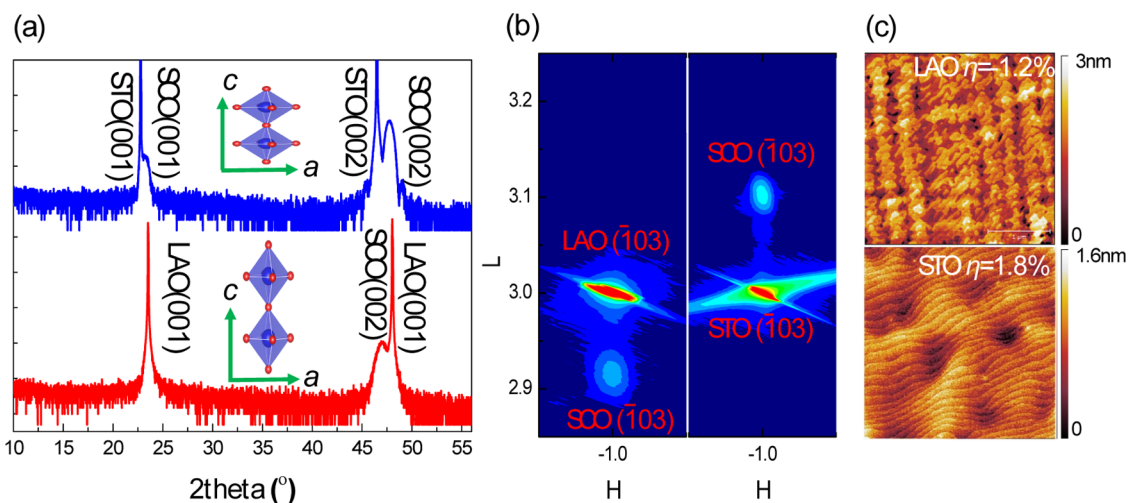
**Figure 1.** (a) XRD $\theta-2\theta$ scans, (b) RSMs, and (c) AFM of SCO thin films grown on LAO and STO substrates. The insets in (a) show qualitatively how the oxygen octahedra in the perovskite structure responds to the epitaxial strain.

energy density increases to $\sim 10^6$ erg/cm$^3$ from zero over an epitaxial-strain interval of just 1.2%. The origins of these magnetic phenomena are grounded in an out-of-plane to in-plane rotation of the easy-magnetization axis induced by an epitaxial-strain variation spanning from moderately compressive, $-1.2\%$, to moderately tensile, $+1.8\%$.

## 2. EXPERIMENTAL AND THEORETICAL METHODS

A Pascal pulsed laser deposition system with a 248 nm wavelength KrF excimer laser was used for the growth of SCO. Substrates of (100) LaAlO$_3$ (LAO) and (100) SrTiO$_3$ (STO) were used to provide different epitaxial strains. Using the formula $\eta = (a - a_0)/a_0$, where $a_0$ is the equilibrium lattice parameter of bulk SCO (cubic, $a_0 = 3.836$ Å) and $a$ is the lattice parameter of the substrate on which the SCO thin film is grown; therefore, the epitaxial strain introduced in the SCO thin films grown on LAO (cubic, $a = 3.789$ Å) is $-1.2\%$ and that introduced in the thin films grown on STO (cubic, $a = 3.905$ Å) is $+1.8\%$.[21] For STO substrates, the growth conditions were temperature of 750 °C, oxygen pressure of 100 mTorr, laser energy density of 4.5 J/cm$^2$, and laser frequency of 1 Hz. After 600 pulses, the thickness of the film was estimated to be 20 nm through X-ray reflectometry measurements. To obtain a perovskite SCO thin film, a postannealing in 600 Torr of oxygen was carried out at 600 °C, then the sample was cooled down to room temperature (RT) at the rate of 30 °C/min without breaking the pressure. However, the direct in situ growth of fully oxidized perovskite SCO on LAO, i.e., postdeposition annealing in high oxygen pressure, is not possible.[21−23] Therefore, we grew the brownmillerite SrCoO$_{3-\delta}$ thin film first and then oxidized it with NaClO solution.[24,25] The growth conditions for the brownmillerite SCO were substrate temperature of 600 °C, oxygen pressure of 50 mTorr, laser energy density of 3 J/cm$^2$, frequency of 1 Hz and 1200 pulses, and then cooling down to RT at the rate of 30 °C/min in 100 mTorr of oxygen. The thickness of the film was 20 nm as determined by X-ray reflection measurements. After that, the thin film was oxidized by a 10 wt % NaClO solution for 10 min. The resulting sample was cleaned ultrasonically twice with deionized water for 5 min and then dried in air. The structures and strain conditions of the as-prepared thin films were characterized by XRD (Bruker D-8). The surface topography was measured by atomic force microscopy (AFM, AIST-NT). The magnetic properties were investigated by MPMS (Quantum Design). The magnetic domain structure of the thin films was characterized by low-temperature MFM at various temperatures (Attocube Attodry 1000). The MFM tips used were CoCr-coated silicon from Mikromasch. The image was obtained with a dual-pass technique, where the lift height was 60 nm for the second pass. The tip was checked before and after the measurement with hard

drive disk reference samples to ensure its functioning during the measurements.

We calculated the zero-temperature energy of stoichiometric SCO thin films in the epitaxial strain interval $-2.5\% \leq \eta \leq +4.5\%$ with first principles methods based on density functional theory (DFT), as it has been proven to be valid in gauging La$_{1-x}$Sr$_x$MnO$_3$.[26] Four different collinear arrangements were considered for the magnetic moments in cobalt atoms: FM (all spins parallel), AFM-A (in-plane spins parallel, out-of-plane spins antiparallel), AFM-G (in-plane spins antiparallel, out-of-plane spins antiparallel), and AFM-C (in-plane spins antiparallel, out-of-plane spins parallel). We used the PBEsol variant of the generalized gradient approximation to DFT[27] as implemented in the Vienna ab initio simulation package.[28,29] We verified that, analogous to what occurs in other oxide cobaltites,[30] the PBEsol functional provides a better description of the magnetic properties of the system, as compared to the experiments, than PBE (see the Supporting Information Figure S3). A "Hubbard-$U$" scheme with $U = 6.0$ eV was employed for a better treatment of the Co's 3d electrons.[16] We used the "projector augmented wave" method to represent the ionic cores[31] and considered the following electrons as valence: Sr's 4s, 4p, and 5s; Co's 3p, 4s, and 3d; and O's 2s and 2p. Wave functions were represented in a plane-wave basis truncated at 650 eV, and we used a 20 atom $\sqrt{2} \times \sqrt{2} \times 2$ simulation cell that allows to reproduce the usual ferroelectric and anti-ferrodistortive distortions in perovskite oxides.[32,33] For integrations within the first Brillouin zone, we employed a $\Gamma$-centered $k$-point grid of $8 \times 8 \times 8$. Geometry relaxations were performed by using a conjugate-gradient algorithm that changed the volume and shape of the unit cell (while fulfilling the lattice vector constraints defining thin films), and the imposed tolerance on the atomic forces was of 0.01 eV/Å. By using these parameters, we obtained total energies that were converged to within 0.5 meV per formula unit. We note that in our DFT calculations, a lattice parameter of $a_0^{\text{DFT}} = 3.89$ Å is estimated for bulk SCO at equilibrium, which, as usual, differs slightly from the corresponding experimental value ($a_0 = 3.84$ Å); we consistently use $a_0^{\text{DFT}}$ in our DFT simulations for estimating the corresponding epitaxial strain conditions.

To simulate the effects of thermal excitations on the magnetic order of SCO thin films, we constructed a Heisenberg spin model of the form $H = E_0 + 1/2\sum_{\langle ij \rangle} J_{ij}S_iS_j$, where $E_0$ represents a constant, $S_i$ represents the magnetic moment of the $i$th atom, and the values of the exchange constants $J_{ij}$ are obtained from zero-temperature DFT energy calculations; we note that only magnetic interactions between nearest neighbor spins are considered. We used this model to perform Monte Carlo (MC) simulations in a periodically repeated simulation box containing $20 \times 20 \times 20$ spins. Thermal averages were computed from runs of 50 000 MC sweeps after equilibration. These simulations

allowed us to monitor the temperature-dependence of the magnetic order through the computation of the ferromagnetic order parameter $S^{FM} = 1/N\sum_i S_{iz}$, where $N$ is the total number of spins in the simulation box. We note that for the calculation of $S^{FM}$, we considered only the z-component of the spins because a small symmetry-breaking magnetic anisotropy was introduced in the system to facilitate the analysis of the results.[30,34]

## 3. RESULTS AND DISCUSSION

**3.1. Crystal Structure and Surface Topography.** The structures and surface topography of the thin films were characterized by XRD and AFM, respectively. Figure 1a shows the XRD $\theta-2\theta$ scans for SCO thin films grown on (001) STO and LAO substrates. Because of the compressive strain, the SCO(002) peak locates on the left of LAO(002) but shifts to the right of STO(002) due to tensile strain. No phases of impurities or half-order peaks were detected, which implies that we have obtained pure perovskite SCO thin films. It is noted that the peak intensity of the film on LAO is lower than that on STO. This probably arises from the twinning feature of the LAO crystal, as only part of it takes part in the diffraction on the one hand; on the other hand, the layer-plus-island surface structure reduces the surface smoothness and crystallinity of the thin film. The strain state of the thin films was investigated by reciprocal space maps (RSMs), which are shown in Figure 1b. No horizontal shift was observed between either LAO($\bar{1}$03) or STO($\bar{1}$03) and SCO($\bar{1}$03), demonstrating that our thin films are fully strained by the substrates and no relaxation between SCO and the substrates. No diffusion in transverse or longitudinal direction for SCO($\bar{1}$03) spots were observed, implying that our films were coherent in both in-plane and out-of-plane directions, with no lattice relaxation in either directions. This is important in later discussion, as we can exclude effects from impurity phases and grain boundaries, which can act as pinning centers during magnetization.[35,36]

Figure 1c gives the surface topography measured by AFM. Both samples exhibit very smooth surfaces over a 3 × 3 $\mu$m$^2$ scan range, with visible 4 Å terraces, whose root mean square roughnesses are 0.3 and 0.2 nm for SCO/LAO and SCO/STO, respectively. These surface topographies are essential in excluding artificial features due to crosstalk between the topography and the MFM.

**3.2. Magnetization Measurements.** The temperature-dependent magnetization of the thin films was then measured by SQUID magnetometry (MPMS). Figure 2a shows the field cool down M–T curves with sample surface perpendicular ($\perp$) and parallel ($\parallel$) to the applied magnetic field. A small field of 100 Oe was applied during the measurement. The thin films became ferromagnetic while decreasing the temperature in either out-of-plane or in-plane directions. In the normal direction, the $T_c$ for SCO/LAO was approximately 250 K and decreased to 170 K on STO. Note that the $T_c$ was estimated by extrapolating the linear part of the M–T curves below the ferromagnetic phase transition to its paramagnetic background. It seems that driving the strain to the compressive side would help to increase the $T_c$. This phenomenon could be explained by our theoretical calculations in Figure 5d, in which the evolution of the Curie temperature, $T_c$, as a function of epitaxial strain are enclosed. As can be observed therein, by increasing the epitaxial strain within the interval $-2.5\% \leq \eta \leq +3.5\%$, the value of $T_c$ is decreased almost linearly. Our results also demonstrate that SCO is ferromagnetic at moderate compressive strains. The mixture of ferromagnetic and
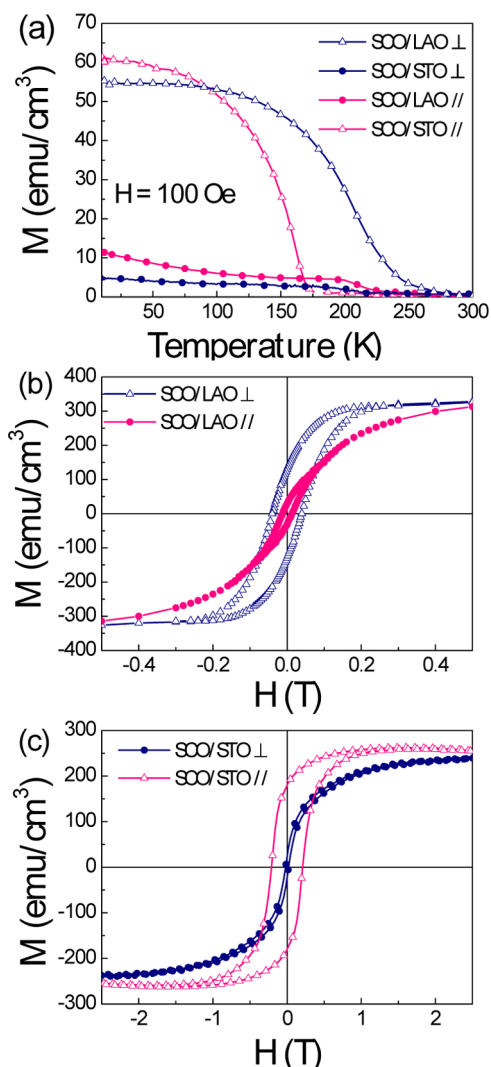


**Figure 2.** (a) Temperature-dependent magnetization of SCO thin films on LAO and STO substrates measured along perpendicular ($\perp$) and parallel ($\parallel$) directions. A small magnetic field of 100 Oe was applied during the measurement. The magnetic hysteresis loops at 10 K on LAO and STO are given in (b) and (c), respectively.
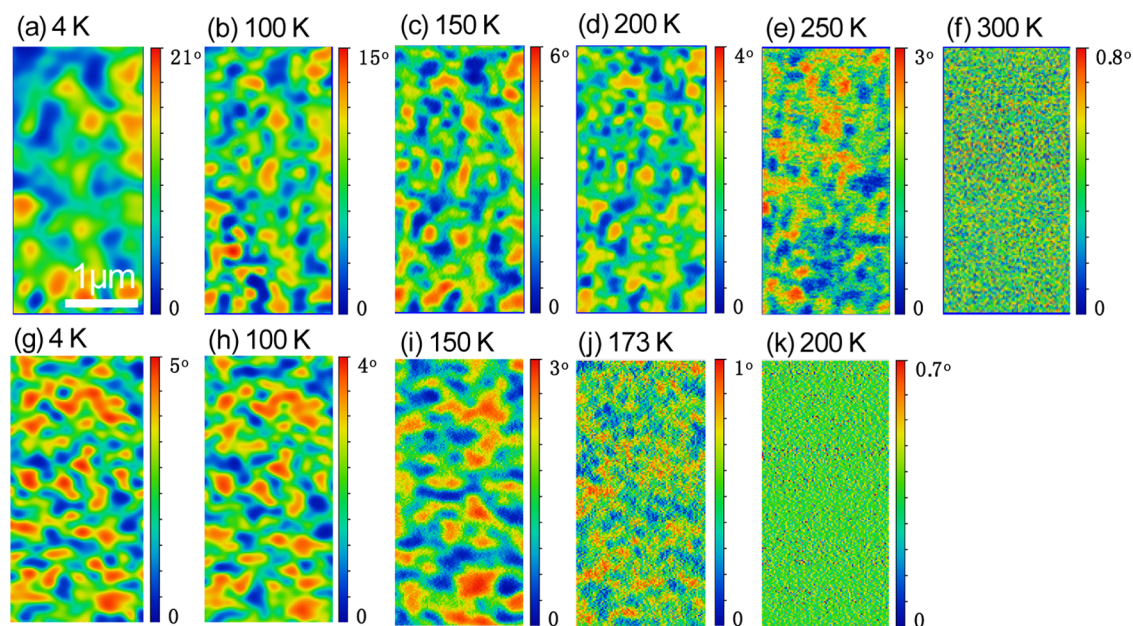
antiferromagnetic phases in a previous report probably arises from the brownmillerite impurity resulting from the employed preparation method.[37] The most fascinating point was that the easy axis of SCO thin film on STO was rotated to the out-of-plane direction by simply changing the LAO substrate, which means a large magnetic anisotropy could be realized by epitaxial strain. Similar phenomena have been observed for La$_{0.7}$Sr$_{0.3}$MnO$_3$ thin films;[3] however, this is the first report for SCO.

Direct evidence of strain-controlled giant magnetic anisotropy is given in Figure 2b,c by the magnetic hysteresis loops of SCO thin films on LAO and STO substrates. The saturation magnetization ($M_s$) for SCO thin films on LAO and STO are approximately 300 and 250 emu/cm$^3$, respectively. In bulk SCO$_{3.0}$, a total moment of 2.5 $\mu_B$/fu (~300 emu/cm$^3$) has been observed.[17] The difference in $M_s$ probably stems from the exchange constants distinction between the parallel and the perpendicular directions.

As shown in Figure 5c, the perpendicular direction has much larger exchange constants, which enhanced the $M_s$ for SCO on

**Table 1. Perpendicular Magnetic Anisotropy Energy Density and Other Physical Properties of Some Oxide Materials Displaying PMA**

| material | $Y_3Fe_5O_{12}$[7] | $Tm_3Fe_5O_{12}$[6] | $Sr_2FeMoO_6$[5] | $SrCoO_{3-\delta}$ | $CoFe_2O_4$[4,40] |
|---|---|---|---|---|---|
| $K_u$ ($10^5$ erg/cm$^3$) | 0.27 | 1.19 | 2.81 | 7.65 | 40−60 |
| structure | garnet | garnet | double perovskite | perovskite | spinel |
| conductance type | dielectric ∼ 0 | dielectric ∼ 0 | semi-metal | metallic | dielectric ∼ 0 |



**Figure 3.** Evolution of magnetic domains observed in MFM measurements by heating SCO thin films through the Curie point. (a−f) SCO on LAO substrate and (g−k) on STO substrate. The sample was prepared by cooling down in zero field. All the images were obtained in the absence of external magnetic field.

LAO. Comparing Figure 2b with 2c, the easy axis of SCO thin film was rotated to the in-plane direction by tensile strain or to the out-of-plane direction by compressive strain, indicating that the shape anisotropy is overwhelmed by the magneto-crystalline anisotropy, which tends to lay the easy axis along the out-of-plane direction. Note that the easy axis of bulk SCO is in [111] direction, and the anisotropy is fairly small along different axis.[17] This result is consistent with the $M-T$ curves shown in Figure 2a. It is found that in tensile-strained SCO/STO, the in-plane magnetization saturates at a smaller magnetic field than that along the out-of-plane; however, in the compressive strained SCO/LAO, the out-of-plane magnetization saturates first. Such a behavior indicates that PMA is successfully achieved in SCO thin films through epitaxial strain. The anisotropy energy density may be calculated as

$$K_u = M_s H_k / 2 \tag{1}$$

where $M_s$ is the saturation magnetization and $H_k$ is the anisotropy field obtained from the extrapolated intersection of the magnetization curve in the parallel direction with that in the normal direction.[38,39] To make a comparison, we summarize $K_u$ of some known complex oxides exhibiting PMA in Table 1.

Although $K_u$ of SCO is smaller than that of $CoFe_2O_4$, it is significantly larger than the previously claimed "giant" 2.81 × $10^5$ erg/cm$^3$ in double perovskite $Sr_2FeMoO_6$ thin films, the 1.19 × $10^5$ erg/cm$^3$ in garnet $Tm_3Fe_5O_{12}$, and the 0.27 × $10^5$ erg/cm$^3$ in $Y_3Fe_5O_{12}$. Such a giant perpendicular anisotropy

makes SCO a potential candidate for high-density data storage and spintronics applications.

**3.3. MFM.** The evolution of temperature-dependent magnetization was further evidenced by MFM. The results are given in Figure 3. MFM is a powerful tool for visualizing the magnetic domains at various temperatures.[41,42] The perpendicular component of stray field from the thin film is sensed by an interferometer through a magnetic tip. Therefore, for films with PMA, the MFM is most sensitive to the domains themselves, whereas for films with in-plane easy axis, the MFM is most sensitive to the domain walls. In a noncontact mode, the tip was tuned to its resonance frequency before the measurement, at which the phase was defined as zero. As a magnetic tip scans across a multidomain surface, the variance of the local magnetic stray field would attract or release the tip, which results in the contrast in the output phase image. Figure 3a−f shows the evolution of MFM for SCO thin film on LAO. These images were carefully aligned to the same location according to the topography features of the scanned area. As mentioned above, on LAO substrate, the image contrast originates from the magnetic domains, whereas on STO, it reflects the distribution of domain walls. Unlike the stripe domains in a hard drive disk or Co/Pt multilayers,[43,44] the domains on the LAO shape in nonuniform clusters. The magnitude of magnetic domain contrast reduces gradually as the temperature increases by looking at the scale bars. When the sample was heated up to above $T_c$, the magnetic domains totally disappeared. This trend is consistent with the previous magnetization measurements shown in Figure 2a. Interestingly,
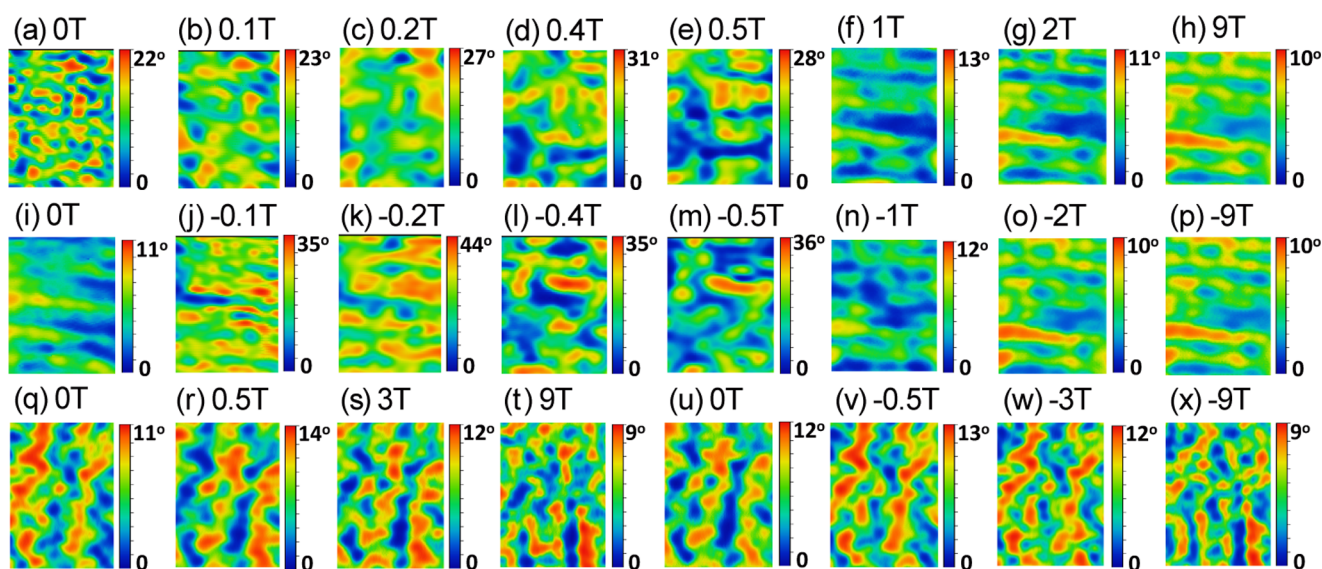
**Figure 4.** Evolution of magnetic domains with external magnetic field. MFM measurements on SCO thin films for (a)−(p) on LAO substrate and (q)−(x) on STO substrate. All the images were obtained at 10 K with magnetic field perpendicular to the sample surface.

on STO substrate, the MFM phase contrast (see Figure 3g−k) was clearly observed as well. The only explanation would be that it is Bloch wall rather than Néel wall that separates the in-plane magnetic domains. It seems that on the STO substrate, the size and density of domain walls do not change much with temperature, indicating no countable new domains are formed during the heating up. Therefore, it is the thermal excitation that ruins the spontaneous polarization and suppresses the net moment, which is not surprising for all magnets. However, on LAO substrates, it was found that the size of the domain decreases continuously with temperature. Unlike on STO, the SCO on LAO tends to form new domains/domain walls locally to accommodate the thermal excitation, rather than solely ruining the magnetic polarization for all of them.

Correspondingly, the evolution of magnetic domains by varying the applied magnetic field was visualized by MFM. The results are shown in Figure 4. The top panel in Figure 4a−h was captured for SCO/LAO by increasing the perpendicular field from 0 to 9 T. The magnetic domains grew up by comparing part (a) with (b), which means some of the domains under spontaneous polarization were aligned to the direction of an external field. Such a tendency was maintained up to 0.2 T, at which point the out-of-plane magnetization was saturated. Note that the contrast in Figure 4c was reversed due to the tip polarity flips. It is expected that the magnetic domains would disappear by further increasing the magnetic field; however, strong contrast was still observed at 0.4 T even up to 0.5 T. Such a manifestation may arise from the PMA of the thin film. The magnetization in out-of-plane direction saturates before it does in the in-plane direction, thus the observed phase contrast actually reflects the domain walls of the in-plane domains. However, these MFM contrast lost finally as the magnetization is saturated in both directions. The stripy contrast diminished in magnitude in Figure 4f,g corresponds to the surface topography shown in Figure 1c.

After reaching a maximum of 9 T, we swapped the field direction. The results are shown in Figure 4i−p. At 0 T, the thin film did not recover completely to the magnetic multidomain state but maintained most of the stripy features as that at 9 T. That means the multidomain structures in the

SCO thin film on LAO did not engender spontaneously after being exposed to a large field. Such a phenomenon was probably attributed to the pinning effect of the substrate, which hindered the rotation of magnetic moment. The multidomain structures started to form as the pinning effect was overwhelmed by applying a small reverse field, see Figure 4j. However, the overall pattern looks quite different from that at the first polarization in Figure 4b. Our measurement upon the second polarization (see Figure S2 of the Supporting Information) exhibited very similar feature with Figure 4j, indicating that the initial domain state under spontaneous polarization may not be recovered as a result of renucleation. Further increasing of the negative magnetic field shows similar trend as those along the positive direction.

The MFM phase contrast for SCO/STO is shown in Figure 4q−x. Comparing the images of the two substrates, the magnitude of MFM signals from SCO/LAO (22−44°) is much larger than that of the signals from SCO/STO (9−14°). As mentioned previously, the observed contrast at 0 T arises actually from the Bloch wall of the in-plane magnetic domains. Thus, the direct measurement of the in-plane magnetic domains is not possible. However, we can estimate the domain configuration through the domain walls distribution. Qualitatively, they were quite similar to each other, as the in-plane direction of SCO/STO is in fact equivalent to the out-of-plane direction of SCO/LAO in the sense of strain. At 0.5 T, the contrast in (q) reversed completely as the tip polarity flips. However, a small difference can be found at 3 T or even up to 9 T. It seems that these domain walls were quite robust against the perpendicular field, reflecting the extremely stable in-plane magnetic domains in tensile strained SCO thin films. Such a behavior may be related to the paramagnetic-like nature in the perpendicular direction, as shown in Figure 2c. Therefore, the polarization of magnetic domains to the out-of-plane direction was strictly prohibited. However, the magnetic domain walls can be slightly aligned as indicated by the scale bars. An analogous trend can be found for down field in Figure 4u−x.

**3.4. DFT Calculations.** To microscopically understand the cause behind the observed magnetic anisotropy in SCO thin films, we performed extensive spin-polarized DFT calculations
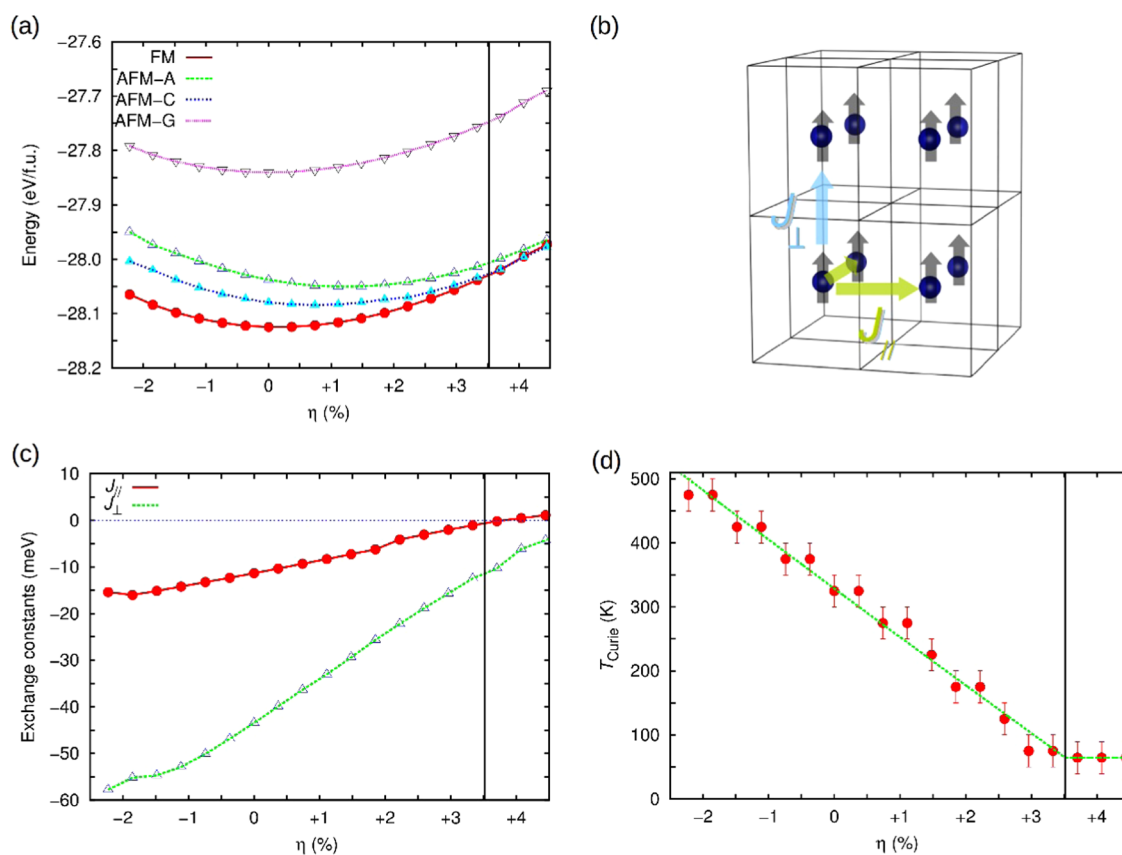
**Figure 5.** Results and details of DFT and MC Heisenberg spin model calculations performed in SCO thin films. (a) Zero-temperature DFT energy expressed as a function of epitaxial strain and collinear spin arrangement. The vertical line indicates the occurrence of a magnetic phase transition. (b) Sketch of $J_{\parallel}$ and $J_{\perp}$ exchange constants defining our Heisenberg spin model. (c) Value of $J_{\parallel}$ and $J_{\perp}$ exchange constants obtained from DFT calculations and expressed as a function of epitaxial strain. (d) Critical Curie temperature obtained from MC Heisenberg spin model simulations and expressed as a function of epitaxial strain.

based on the PBEsol functional (see Section 2 for technical details). In Figure 5a, we show the zero-temperature energy of the four considered collinear spin arrangements expressed as a function of epitaxial strain, $\eta$. As observed therein, our first principles calculations render a FM → AFM-C magnetic phase transition at a tensile strain of $\eta_c$ = +3.5%, which is in qualitative agreement with the experiments reported in the literature. We note, however, that the value of the predicted critical strain is quite sensitive to the choice of the DFT exchange−correlation functional (e.g., $\eta_c$ turns out to be +2.0% when using the PBE functional[16]).

We constructed a Heisenberg spin model based on the zero-temperature DFT results presented in Figure 5a (see Section 2 for technical details). Specifically, we considered the magnetic exchange interactions among the nearest neighboring Co atoms and made a distinction between in-plane ($\parallel$) and out-of-plane ($\perp$) interactions (see Figure 5b). The value of the corresponding $J_{\parallel}$ and $J_{\perp}$ exchange constants, which quantify the strength of the magnetic interactions along the parallel and normal directions, respectively, then can be easily estimated as

$$J_{\parallel}(\eta) = 1/4(E^{FM} - E^{AFM\text{-}C}) \tag{2}$$

$$J_{\perp}(\eta) = 1/2(E^{FM} - E^{AFM\text{-}A}) \tag{3}$$

where their dependence on the epitaxial strain has been explicitly noted. We enclose our $J_{\parallel}$ and $J_{\perp}$ exchange constant results in Figure 5c. As can be observed therein, at moderate

compressive strains ($\eta$ = −2%), the magnetic interactions along the normal direction are much more intense than along the parallel direction, which indicates the presence of a marked magnetic anisotropy in the system. As we move toward tensile strains, both exchange constants undergo a significant reduction, specially $J_{\perp}$. This result suggests a $\eta$-induced reduction of the Curie temperature in SCO thin films when moving from compressive to tensile strains, which is fully consistent with our observations. In all the analyzed cases, the absolute value of $J_{\perp}$ is larger than that of $J_{\parallel}$, thus implying that ferromagnetic spin order along the normal direction will endure further than along the parallel direction at high temperatures. These results are in coherent agreement with our experiments performed in LAO and SCO substrates, which respectively introduce an epitaxial strain of −1.2 and +1.8% in SCO.

To explicitly reproduce the effects of the thermal excitations on the magnetic order of SCO thin films, we performed a series of Monte Carlo simulations based on the described Heisenberg spin model. By monitoring the evolution of the ferromagnetic order parameter as a function of temperature, we could determine the corresponding Curie temperature, $T_c$, as a function of epitaxial strain; our results are enclosed in Figure 5d. As can be observed therein, by increasing the epitaxial strain within the interval $-2.5\% \leq \eta \leq +3.5\%$, the value of $T_c$ is decreased almost linearly. Specifically, for a compressive strain of −1.2%, we estimate a Curie temperature of 425 ± 50 K and for +1.8%, we obtain 200 ± 50 K. These

results are qualitatively in good agreement with our $T_c$ measurements performed in LAO and SCO substrates (see Figure 2).

## 4. CONCLUSIONS

In summary, we have disclosed a giant magnetic anisotropy in high-quality epitaxial SCO thin films that can be efficiently tuned by means of strain. Specifically, the easy magnetization axis in the SCO thin films can be changed from out-of-plane to in-plane by varying the epitaxial strain conditions from moderately compressive (−1.2%, as grown in LAO) to moderately tensile (+1.8%, as grown in STO). Simultaneously, the Curie temperature along the easy magnetization axis increases from 170 to 250 K. The local variance of MFM upon temperature and magnetic field reveals that the evolution of magnetic domains in the SCO thin film is strongly dependent on the epitaxial strains. We showed that the magnetic domain diminished gradually by approaching the Curie temperature. On the STO substrate, the size of magnetic domain remained unchanged. However, on LAO substrates, it decreased continuously to accommodate the thermal excitation rather than solely ruin the magnetic polarization. The field-dependent measurements showed that the MFM signal did not disappear until the anisotropy magnetic field due to PMA of SCO/LAO. The multidomain structures in SCO/LAO did not engender spontaneously after being exposed to a large field due to the pinning effect of the substrate. Although it could be recovered by applying a small reverse field, the overall pattern would be different as a result of renucleation. In SCO/STO, the domain walls were quite robust against the perpendicular field, reflecting extremely stable in-plane magnetic domains in tensile strained SCO thin films. Such a behavior may be related to the paramagnetic-like nature in the perpendicular direction. These experimental results were quantitatively explained by first principles calculations in terms of strain-induced variations in the out-of-plane and in-plane magnetic exchange constants. A PMA with a giant anisotropy energy of ∼$10^6$ erg/cm$^3$ is successfully achieved in the SCO thin film through strain control. Our findings entail the giant magnetic anisotropy so far unseen in a metallic perovskite oxide, which should stimulate the use of SCO nanomaterials in actual high-density data storage and spintronic applications. Further investigations of the magnetic transport properties and magnetic excitations (magnons)[45−48] in this material are highly desirable.

## ASSOCIATED CONTENT

### Ⓢ Supporting Information

The Supporting Information is available free of charge on the ACS Publications website at DOI: 10.1021/acsami.8b03553.

> Temperature-dependent resistivity of perovskite and brownmillerite SCO thin films on LAO and STO substrates; evolution of magnetic domains in SCO/LAO after being exposed to high field; DFT-PBE and MC Heisenberg spin model results obtained in SCO thin films (PDF)

## AUTHOR INFORMATION

### Corresponding Authors

*E-mail: husb@sustc.edu.cn (S.H.).
*E-mail: jan.seidel@unsw.edu.au (J.S.).

### ORCID ⊕

Claudio Cazorla: 0000-0002-6501-4513
Jianbo Wang: 0000-0002-3315-3105
Jan Seidel: 0000-0003-2814-3241

### Notes

The authors declare no competing financial interest.

## ■ ACKNOWLEDGMENTS

## ■ REFERENCES

(1) Suzuki, Y.; Hwang, H. Y. Anisotropy of Magnetoresistance in (110)La$_{0.7}$Sr$_{0.3}$MnO$_3$ Thin Films. *J. Appl. Phys.* **1999**, *85*, 4797−4799.

(2) Nath, T. K.; Rao, R. A.; Lavric, D.; Eom, C. B.; Wu, L.; Tsui, F. Effect of Three-dimensional Strain States on Magnetic Anisotropy of La$_{0.8}$Ca$_{0.2}$MnO$_3$ Epitaxial Thin Films. *Appl. Phys. Lett.* **1999**, *74*, 1615−1617.

(3) Tsui, F.; Smoak, M. C.; Nath, T. K.; Eom, C. B. Strain-dependent Magnetic Phase Diagram of Epitaxial La$_{0.67}$Sr$_{0.33}$MnO$_3$ Thin Films. *Appl. Phys. Lett.* **2000**, *76*, 2421−2423.

(4) Suzuki, Y.; Hu, G.; Van Dover, R. B.; Cava, R. J. Magnetic Anisotropy of Epitaxial Cobalt Ferrite Thin Film. *J. Magn. Magn. Mater.* **1999**, *191*, 1−8.

(5) Du, C.; Adur, R.; Wang, H.; Hauser, A. J.; Yang, F.; Hammel, P. C. Control of Magnetocrystalline Anisotropy by Epitaxial Strain in Double Perovskite Sr$_2$FeMoO$_6$ Films. *Phys. Rev. Lett.* **2013**, *110*, No. 147204.

(6) Quindeau, A.; Avci, C. O.; Liu, W.; Sun, C.; Mann, M.; Tang, A. S.; Onbasli, M. C.; Bono, D.; Voyles, P. M.; Xu, Y.; Robinson, J.; Beach, G. S. D.; Ross, C. A. Tm$_3$Fe$_5$O$_{12}$/Pt Heterostructures with Perpendicular Magnetic Anisotropy for Spintronic Applications. *Adv. Electron. Mater.* **2017**, *3*, No. 1600376.

(7) Fu, J.; Hua, M.; Wen, X.; Xue, M.; Ding, S.; Wang, M.; Yu, P.; Liu, S.; Han, J.; Wang, C.; Du, H.; Yang, Y.; Yang, J. Epitaxial Growth of Y$_3$Fe$_5$O$_{12}$ Thin Films with Perpendicular Magnetic Anisotropy. *Appl. Phys. Lett.* **2017**, *110*, No. 202403.

(8) Perna, P.; Maccariello, D.; Ajejas, F.; Guerrero, R.; Méchin, L.; Flament, S.; Santamaria, J.; Miranda, R.; Camarero, J. Engineering Large Anisotropic Magnetoresistance in La$_{0.67}$Sr$_{0.33}$MnO$_3$ Films at Room Temperature. *Adv. Funct. Mater.* **2017**, *27*, No. 1700664.

(9) Lee, J. H.; Rabe, K. M. Coupled Magnetic-ferroelectric Metal-insulator Transition in Epitaxially Strained SrCoO$_3$ from First Principles. *Phys. Rev. Lett.* **2011**, *107*, No. 067601.

(10) Jeen, H.; Choi, W. S.; Freeland, J. W.; Ohta, H.; Jung, C. U.; Lee, H. N. Topotactic Phase Transformation of the Brownmillerite SrCoO$_{2.5}$ to the Perovskite SrCoO$_{3−δ}$. *Adv. Mater.* **2013**, *25*, 3651−6.

(11) Jeen, H.; Choi, W. S.; Biegalski, M. D.; Folkman, C. M.; Tung, I. C.; Fong, D. D.; Freeland, J. W.; Shin, D.; Ohta, H.; Chisholm, M. F.; Lee, H. N. Reversible Redox Reactions in an Epitaxially Stabilized SrCoO$_x$ Oxygen Sponge. *Nat. Mater.* **2013**, *12*, 1057−1063.

(12) Hu, S.; Yue, Z.; Lim, J. S.; Callori, S. J.; Bertinshaw, J.; Ikeda-Ohno, A.; Ohkochi, T.; Yang, C.-H.; Wang, X.; Ulrich, C.; Seidel, J. Growth and Properties of Fully Strained SrCoO$_x$ (x ≈ 2.8) Thin Films on DyScO$_3$. *Adv. Mater. Interfaces* **2015**, No. 1500012.

(13) Callori, S. J.; Hu, S.; Bertinshaw, J.; Yue, Z. J.; Danilkin, S.; Wang, X. L.; Nagarajan, V.; Klose, F.; Seidel, J.; Ulrich, C. Strain-induced Magnetic Phase Transition in $SrCoO_{3-\delta}$ Thin Films. *Phys. Rev. B* **2015**, *91*, No. 140405(R).

(14) Hoffmann, M.; Borisov, V. S.; Ostanin, S.; Mertig, I.; Hergert, W.; Ernst, A. Magnetic Properties of Defect-free and Oxygen-deficient Cubic $SrCoO_{3-\delta}$. *Phys. Rev. B* **2015**, *92*, No. 094427.

(15) Petrie, J. R.; Mitra, C.; Jeen, H.; Choi, W. S.; Meyer, T. L.; Reboredo, F. A.; Freeland, J. W.; Eres, G.; Lee, H. N. Strain Control of Oxygen Vacancies in Epitaxial Strontium Cobaltite Films. *Adv. Funct. Mater.* **2016**, *26*, 1564−1570.

(16) Rivero, P.; Cazorla, C. Revisiting the Zero-temperature Phase Diagram of Stoichiometric $SrCoO_3$ with First-principles Methods. *Phys. Chem. Chem. Phys.* **2016**, *18*, 30686−30695.

(17) Long, Y.; Kaneko, Y.; Ishiwata, S.; Taguchi, Y.; Tokura, Y. Synthesis of Cubic $SrCoO_3$ Single Crystal and Its Anisotropic Magnetic and Transport Properties. *J. Phys.: Condens. Matter* **2011**, *23*, No. 245601.

(18) Taguchi, H.; Shimada, M.; Koizumi, M. Effect of Oxygen Vacancy on the Magnetic Properties in the System $SrCoO_{3-\delta}$ ($0.5 \leq \delta < 0$). *J. Solid State Chem.* **1979**, *29*, 221−225.

(19) Takeda, Y.; Kanno, R.; Takada, T.; Bando, Y.; Takano, M.; Yamamo, O. Phase Relation and Oxygen-non-stoichiometry of Perovskite-like Compound $SrCoO_x$ ($2.29 < x < 2.80$). *Z. Anorg. Allg. Chem.* **1986**, 259−270.

(20) Takeda, T.; Watanabe, H.; Yamaguchi, Y. Magnetic Structure of $SrCoO_{2.5}$. *J. Phys. Soc. Jpn.* **1972**, *33*, 970−972.

(21) Hu, S.; Wang, Y.; Cazorla, C.; Seidel, J. Strain-Enhanced Oxygen Dynamics and Redox Reversibility in Topotactic $SrCoO_{3-\delta}$ ($0 < \delta \leq 0.5$). *Chem. Mater.* **2017**, *29*, 708−717.

(22) Scullin, M. L.; Yu, C.; Huijben, M.; Mukerjee, S.; Seidel, J.; Zhan, Q.; Moore, J.; Majumdar, A.; Ramesh, R. Anomalously Large Measured Thermoelectric Power Factor in $Sr_{1-x}La_xTiO_3$ Thin Films due to $SrTiO_3$ Substrate Reduction. *Appl. Phys. Lett.* **2008**, *92*, No. 202113.

(23) Scullin, M. L.; Ravichandran, J.; Yu, C.; Huijben, M.; Seidel, J.; Majumdar, A.; Ramesh, R. Pulsed Laser Deposition-induced Reduction of $SrTiO_3$ Crystals. *Acta Mater.* **2010**, *58*, 457−463.

(24) Hu, S.; Seidel, J. Oxygen Content Modulation by Nanoscale Chemical and Electrical Patterning in Epitaxial $SrCoO_{3-\delta}$ ($0 < \delta \leq 0.5$) thin films. *Nanotechnology* **2016**, *27*, No. 325301.

(25) Ichikawa, N.; Iwanowska, M.; Kawai, M.; Calers, C.; Paulus, W.; Shimakawa, Y. Reduction and Oxidation of $SrCoO_{2.5}$ Thin Films at Low Temperatures. *Dalton Trans.* **2012**, *41*, 10507−10510.

(26) Konishi, Y.; Fang, Z.; Izumi, M.; Manako, T.; Kasai, M.; Kuwahara, H.; Kawasaki, M.; Terakura, K.; Tokura, Y. Orbital-state-mediated Phase-control of Manganites. *J. Phys. Soc. Jpn.* **1999**, *68*, 3790−3793.

(27) Perdew, J. P.; Ruzsinszky, A.; Csonka, G. I.; Vydrov, O. A.; Scuseria, G. E.; Constantin, L. A.; Zhou, X.; Burke, K. Restoring the Density-gradient Expansion for Exchange in Solids and Surfaces. *Phys. Rev. Lett.* **2008**, *100*, No. 136406.

(28) Kresse, G.; Furthmuller, J. Efficient Iterative Schemes for Ab Initio Total-energy Calculations Using a Plane-wave Basis Set. *Phys. Rev. B* **1996**, *54*, 11169−11186.

(29) Kresse, G.; Joubert, D. From Ultrasoft Pseudopotentials to the Projector Augmented-wave Method. *Phys. Rev. B* **1999**, *59*, 1758−1775.

(30) Cazorla, C.; Dieguez, O.; Iniguez, J. Multiple Structural Transitions Driven by Spin-phonon Couplings in a Perovskite Oxide. *Sci. Adv.* **2017**, *3*, No. e1700288.

(31) Blöchl, P. E. Projector Augmented-wave Method. *Phys. Rev. B* **1994**, *50*, 17953−17979.

(32) Cazorla, C.; Stengel, M. Ab Initio Design of Charge-mismatched Ferroelectric Superlattices. *Phys. Rev. B* **2014**, *90*, No. 020101.

(33) Cazorla, C.; Stengel, M. Electrostatic Engineering of Strained Ferroelectric Perovskites from First Principles. *Phys. Rev. B* **2015**, *92*, No. 214108.

(34) Cazorla, C.; Iniguez, J. Insights Into the Phase Diagram of Bismuth Ferrite from Quasiharmonic Free-energy Calculations. *Phys. Rev. B* **2013**, *88*, No. 214430.

(35) Angervo, I.; Saloaro, M.; Huhtinen, H.; Paturi, P. Interface Defects Induced Vertical Magnetic Anisotropy in $Sr_2FeMoO_6$ Thin Films. *Appl. Surf. Sci.* **2017**, *422*, 682−689.

(36) Ouarab, N.; Haroun, A. Perpendicular Magnetic Anisotropy in ZnMnS Ultra-thin Films Caused by Structural Cleavage. *J. Magn. Magn. Mater.* **2017**, *443*, 300−308.

(37) Hao, L.; Zhang, Z. F.; Xie, X. N.; Wang, H. R.; Yu, Q. X.; Zhu, H. Preparation of $SrCoO_x$ Thin Films on $LaAlO_3$ Substrate and Their Reversible Redox Process at Moderate Temperatures. *J. Cryst. Growth* **2015**, *427*, 36−41.

(38) Li, X.; Yin, S.; Liu, Y.; Zhang, D.; Xu, X.; Miao, J.; Jiang, Y. Perpendicular Magnetic Anisotropy of Full-Heusler Films in Pt/$Co_2FeAl$/MgO Trilayers. *Appl. Phys. Express* **2011**, *4*, No. 043006.

(39) Carcia, P. F.; Meinhaldt, A. D.; Suna, A. Perpendicular Magnetic Anisotropy in Pd/Co Thin Film Layered Structures. *Appl. Phys. Lett.* **1985**, *47*, 178−180.

(40) Shirsath, S. E.; Liu, X.; Yasukawa, Y.; Li, S.; Morisako, A. Switching of Magnetic Easy-axis Using Crystal Orientation for Large Perpendicular Coercivity in $CoFe_2O_4$ Thin Film. *Sci. Rep.* **2016**, *6*, No. 30074.

(41) Tian, G.; Zhang, F.; Yao, J.; Fan, H.; Li, P.; Li, Z.; Song, X.; Zhang, X.; Qin, M.; Zeng, M.; Zhang, Z.; Yao, J.; Gao, X.; Liu, J. Magnetoelectric Coupling in Well-Ordered Epitaxial $BiFeO_3$/$CoFe_2O_4$/$SrRuO_3$ Heterostructured Nanodot Array. *ACS Nano* **2016**, *10*, 1025−1032.

(42) Zhou, D.; Takahashi, R.; Zhou, Y.; Kim, D.; Suresh, V. K.; Chu, Y.-H.; He, Q.; Munroe, P.; Lippmaa, M.; Seidel, J.; Valanoor, N. Magnetic and Magnetodielectric Properties of Epitaxial Iron Vanadate Thin Films. *Adv. Electron. Mater.* **2017**, *3*, No. 1600295.

(43) Guo, L.; Wang, Y.; Wang, J.; Muraishi, S.; Sannomiya, T.; Nakamura, Y.; Shi, J. Magnetoelastically Induced Perpendicular Magnetic Anisotropy and Perpendicular Exchange Bias of CoO/CoPt Multilayer Films. *J. Magn. Magn. Mater.* **2015**, *394*, 349−353.

(44) Talapatra, A.; Mohanty, J. Laser Induced Local Modification of Magnetic Domain in Co/Pt Multilayer. *J. Magn. Magn. Mater.* **2016**, *418*, 224−230.

(45) Ramirez, M. O.; Krishnamurthi, M.; Denev, S.; Kumar, A.; Yang, S.-Y.; Chu, Y.-H.; Saiz, E.; Seidel, J.; Pyatakov, A. P.; Bush, A.; Viehland, D.; Orenstein, J.; Ramesh, R.; Gopalan, V. Two-phonon Coupling to the Antiferromagnetic Phase Transition in Multiferroic $BiFeO_3$. *Appl. Phys Lett.* **2008**, *92*, No. 022511.

(46) Ramirez, M. O.; Kumar, A.; Denev, S. A.; Chu, Y. H.; Seidel, J.; Martin, L. W.; Yang, S. Y.; Rai, R. C.; Xue, X. S.; Ihlefeld, J. F.; Podraza, N. J.; Saiz, E.; Lee, S.; Klug, J.; Cheong, S. W.; Bedzyk, M. J.; Auciello, O.; Schlom, D. G.; Orenstein, J.; Ramesh, R.; Musfeldt, J. L.; Litvinchuk, A. P.; Gopalan, V. Spin-charge-lattice Coupling through Resonant Multimagnon Excitations in Multiferroic $BiFeO_3$. *Appl. Phys Lett.* **2009**, *94*, No. 161905.

(47) Ramirez, M. O.; Kumar, A.; Denev, S. A.; Podraza, N. J.; Xu, X. S.; Rai, R. C.; Chu, Y. H.; Seidel, J.; Martin, L. W.; Yang, S. Y.; Saiz, E.; Ihlefeld, J. F.; Lee, S.; Klug, J.; Cheong, S. W.; Bedzyk, M. J.; Auciello, O.; Schlom, D. G.; Ramesh, R.; Orenstein, J.; Musfeldt, J. L.; Gopalan, V. Magnon Sidebands and Spin-charge Coupling in Bismuth Ferrite Probed by Nonlinear Optical Spectroscopy. *Phys. Rev. B* **2009**, *79*, No. 224106.

(48) Langner, M. C.; Kantner, C. L. S.; Chu, Y. H.; Martin, L. M.; Yu, P.; Seidel, J.; Ramesh, R.; Orenstein, J. Observation of Ferromagnetic Resonance in $SrRuO_3$ by the Time-Resolved Magneto-Optical Kerr Effect. *Phys. Rev. Lett.* **2009**, *102*, No. 177601.